Al-Azhar Engineering 16th International Conference

Vol. 19, No. 72, July 2024, 92 - 104

DESIGN OF AN EFFICIENT SPIRAL WOUND REVERSE OSMOSIS MEMBRANE

Hamza Abogharraf[1*], Heba Abdallah[2], Said M. A.Ibrahim[1]

[1]Mechanical Engineering Department, Faculty of Engineering, Al-Azhar University, Cairo, Egypt.

[2]Chemical Engineering and Pilot Plant Department, Engineering and Renewable Energy Research Institute, National Research Centre (NRC), Giza, Egypt.

***Correspondence:** hamza.abogharraf@hotmail.com

Citation:

H. Abogharraf, H. Abdallah and S.M.A. Ibrahim, "Design of an efficient spiral wound reverse osmosis membrane", Journal of Al-Azhar University Engineering Sector, vol. 19, pp. 92 - 104, 2024.

Received: 26 November 2023

Revised: 27 December 2023

Accepted: 02 January 2024

DOI:10.21608/auej.2024.251260.1489

ABSTRACT

Since its invention, spiral wound (SW) membrane geometry design has not undergone many significant changes. The conventional design consists primarily of two rectangular membrane leaves sandwiching a feed spacer and rolled over a permeate tube. The significant energy requirement for reverse osmosis, largely utilized to generate the pressure necessary to overcome the osmotic pressure and the pressure drop within the SW membrane, presents a considerable challenge. A significant portion of this energy is dissipated when the fluid traverses the restrictive feed spacer. Numerous studies have been conducted to improve the hydrodynamics of the feed spacer, to mitigate concentration polarization and enhancing overall system efficiency .In this paper a novel SW membrane design is investigated using CFD. 2D and 3D models of SW membrane were constructed to validate against published experimental data under various operational conditions. The model is then used to explore irregular shapes for the membrane leaf as an alternative to the conventional rectangular design. A comparison was made between the traditional rectangular shape and irregular shapes that have the same membrane area. Promising results were obtained for the new design, which also provides an easy to implement remedy for fouling and self-cleaning in SW membranes. Crucially, this innovative design introduces a new factor that can positively influence restrictive criteria controlling SW membrane design optimization

KEYWORDS: Reverse osmosis, Spiral wound membrane, Computational fluid dynamics CFD, desalination, Fouling

تصميم غشاء تناضح عكسي حلزوني كفوء

حمزة ابوغراف[1*], هبة عبدالله[2], سعيد ابراهيم[1]

[1]قسم الهندسة الميكانيكية، كلية الهندسة، جامعة الازهر

[2]قسم الهندسة الكيميائية والتجارب نصف الصناعية، معهد بحوث الهندسة والطاقة المتجددة، المركز القومي للبحوث، الجيزة، مصر.

*البريد الاليكتروني للباحث الرئيسي : hamza.abogharraf@hotmail.com

الملخص

منذ اختراعه، لم يخضع التصميم الهندسي لغشاء التناضح العكسي الحلزوني للعديد من التغييرات المهمة. بشكل أساسي يتكون التصميم التقليدي من ورقتين غشائيتين مستطيلتين وبينهما فاصل تغذية حيث يتم لفهما فوق أنبوب تجميع المياه العدبة. تمثل متطلبات الطاقة الكبيرة للتناضح العكسي تحديًا كبيرًا ، تستهلك اغلب هذه الطاقة في توليد الضغط اللازم للتغلب على الضغط الأسموزي وانخفاض الضغط داخل الغشاء. يتم تبديد جزء كبير من هذه الطاقة عندما يعبر السائل علي فاصل

التغذية المتشابك الشكل . اجريت العديد من الدراسات لتحسين الديناميكا المائية لفاصل التغذية، لتقليل من استقطاب التركيز(concentration polarization) وتعزيز كفاءة النظام بشكل عام. في هذا البحث تم دراسة تصميم جديد للغشاء باستخدام تقنية المحاكاة . تم إنشاء نماذج ثنائية وثلاثية الأبعاد للغشاء والتحقق منها وذلك بمحاكاة تجارب عملية تم نشرها وذلك في ظل ظروف تشغيلية مختلفة. وقد استخدمت هذه النمادج بعد ذلك في استكشاف اشكال غير منتظمة للورقة الغشائية كبديل للتصميم المستطيل التقليدي. وتمت المقارنة بين الشكل المستطيل التقليدي والأشكال غير المنتظمة و وذلك لنفس مساحة الورقة. تم الحصول على نتائج واعدة للتصميم الجديد، الذي يوفر أيضًا وسيلة سهلة التنفيذ لمعالجمة الترسيب والتنظيف الذاتي للغشاء. والأهم من ذلك، أن هذا التصميم المبتكر يقدم عاملاً جديدًا يمكن أن يؤثر بشكل إيجابي على المعايير التقييدية التي تتحكم في تحسين تصميم الغشاء.

الكلمات المفتاحية : التناضح العكسي، اغشية التناضح العكسي الحلزونية، ديناميكا المـوائع الحـسابية، تحلية مياه البحر، الترسيب

1. INTRODUCTION

Due to its characteristic of providing a high surface area to volume ratio and cost, effective spiral wound membrane modules are widely used in a variety of industrial applications such as water desalination and waste water treatment, food and beverage processing, and pharmaceutical manufacturing applications where large volumes of liquids need to be filtered [1]. As Fig. **1** depicts, the spiral wound membrane which is basically a two rectangular flat sheets of membranes separated by mesh spacer glued from all sides except the side connected to a pipe forming an enclosed fabric-like permeating channel called a leaf . Multi leaves sandwiching the feed spacer are wrapped tightly around the permeate tube creating another spiral-like feed channel. The module is placed inside a tubular pressure vessel. Feed passes axially down the module across the membrane leaf. Feed permeates into the membrane leaf, where it spirals towards the center and exits through the collection tube, permeating spacer and pipe. To a certain degree, each component of the module affects the performance SW module. Since the introduction of SW module, numerous experimental and theoretical studies have been conducted to examine that effect. In recent years, the advancement of computational power has led to heightened research interest in exploring the impact of membrane geometry on hydrodynamics and the overall performance of SW modules by computational fluid dynamics (CFD), specifically in relation to concentration polarization, fouling, and scaling mitigation. In a previous study [2], the impact of feed spacer spacing was investigated using CFD. It was observed that the mass transfer capacity increased when the spacer spacing was decreased, but it also led to higher pressure drop and energy consumption. Conversely, increasing the spacer spacing resulted in reduced pressure drop but intensified concentration polarization. Therefore, the selection of optimal spacer spacing should consider both mass transfer capacity and energy consumption. .In another investigation [3], CFD simulations were conducted to compare the performance of circular, triangular, and rectangular spacers under similar pressure conditions. It was found that triangular spacers were capable of generating vortices at lower Reynolds numbers, while circular filaments exhibited lower pressure drop compared to rectangular spacers at equivalent Reynolds numbers. Fluid flow and mass transfer at various Reynolds numbers were explored in previous studies [4 - 5] using non-steady-state laminar flow modeling and CFD simulations. Additionally, the influence of different internal angles and filament angles on the fluid flow within the membrane flow channel was examined.

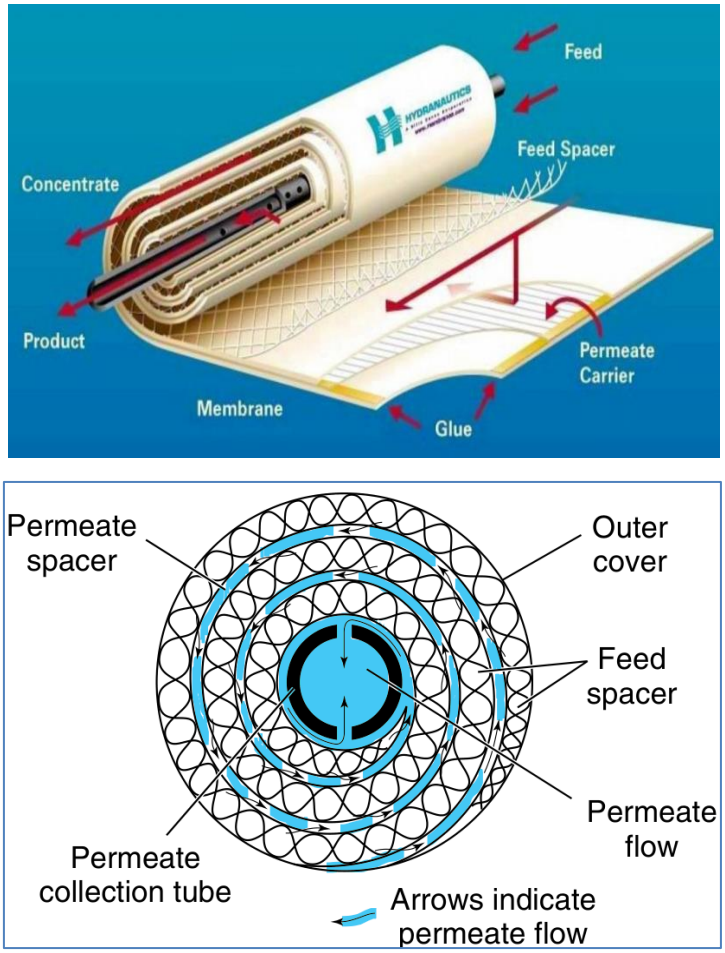

Fig. 1. Spiral wound membrane

In a study [6], a full-scale Reverse Osmosis (RO) module was analyzed using CFD to understand the differences in flow velocities and mass transfer with and without a feed spacer.The effect of airfoil-shaped spacer attack angle was investigated through CFD simulations in previous research [7], and it was found that the suggested airfoil spacer outperformed the commercial spacer. A 2D model was established in a study [8] to examine the effect of using alternating strand diameters of the feed spacer on the Spiral-Wound (SW) module. The results indicated that such a spacer design created a converging-diverging channel, enhancing the mixing of the bulk flow and reducing concentration polarization. It is worth noting that the majority of studies have been directed toward investigating the influence of feed spacer geometry in SW membranes, as it is the component with the most significant impact on concentration polarization and fouling, thus membrane lifespan, and overall performance.

The present work presents a novel design of an SW in which the influence of feed velocity modification through changes in the leaf shape on the performance of the membrane is examined using CFD. The evaluation of these changes excludes the influence of feed spacer, to allow for a separate assessment.

2. MODEL DEVELOPMENT

Owing to its simplicity and its ability to validate experimental data, the flat rectangular channel model is a well-accepted model for spiral wound membranes in the literature [9]. The SW membrane is assumed to be unwounded to form a rectangular channel with constant height H as **Fig**. **2** shows.

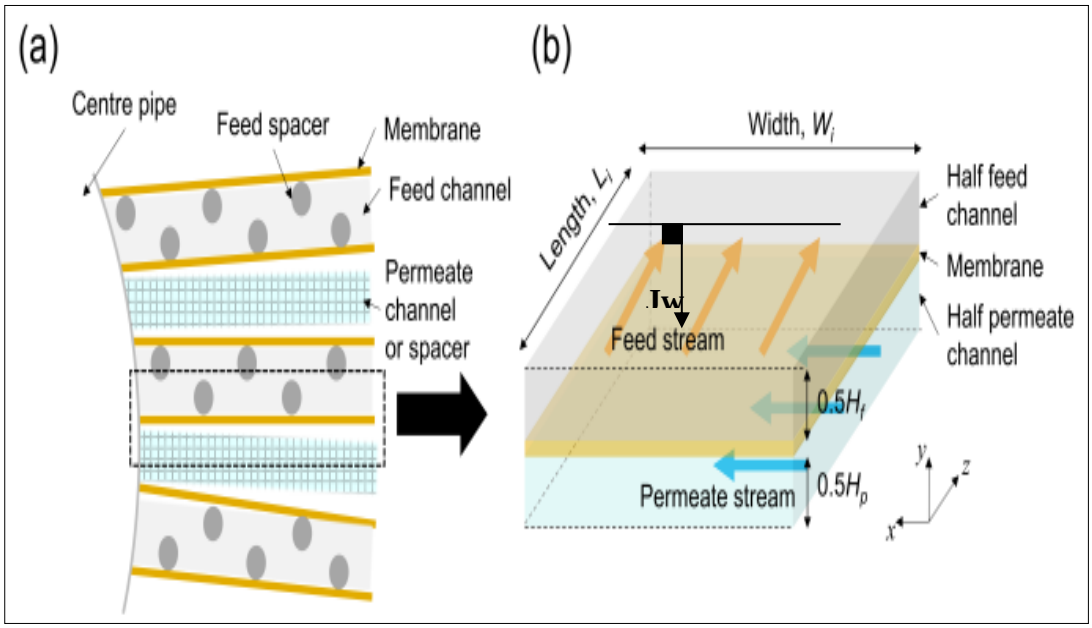

Fig. 2. SW membrane (a) wounded (b) unwounded

2.1 The Governing Equations

In this research, the flow within the spiral wound membrane is assumed to be steady and laminar. This is justified as turbulence is unlikely to occur in SW membranes due to narrow feed channels and relatively low flow velocities of less than 0.5 m/s [9]. Therefore, the flow in SW membranes can be assumed laminar and the corresponding governing equations consist of continuity, Navier-Stokes, and convection-diffusion equations as follows

$$\nabla u = 0 \tag{1}$$

$$\rho u \,.\nabla u = \, -\nabla p + \mu \nabla^2 \, u \tag{2}$$

$$\nabla.\,(D_s \,\nabla u) - \nabla \,.\,(uc) = 0 \tag{3}$$

where u is the flow velocity vector, ρ the density, μ the dynamic viscosity, p the pressure, c the concentration, and Ds the diffusivity.

To accurately predict the membrane performance, it is essential to use realistic boundary conditions that honor the operation condition and the actual SW membrane. Consequently, a fully developed flow and constant salt concentration are imposed at the inlet, and the outlet is kept under the constant gauge pressure. No slip velocity boundary at all walls is considered. To simulate water and salt fluxes through walls that represent the membrane, the most widely accepted solution-diffusion model is incorporated. In this model, the membrane is treated as nonporous and driving mechanisms are the pressure and the concentration difference [10]. To simplify calculations, two assumptions are made: (i) the pressure and concentration in the permeate channel is constant, which is justified as they do not change greatly inside the permeate channel, and (ii) the solute concentration at the wall is not influenced by cross flow which is also justified as the permeate flow rate is less than 10% of the feed [11]. The solution –diffusion model can be expressed as

$$Jw = A(\Delta p - k\Delta c) \tag{4}$$

$$Js = B\Delta c \tag{5}$$

$$Cp = \frac{Js}{Jw} \tag{6}$$

Where Jw is the water flux, Js the solute flux, A the hydraulic conductivity, K the osmotic factor which is constant under isothermal conditions, B the solute permeability, and Δc and Δp are the pressure and concentration difference between feed and permeate, respectively.
It is also reasonable to assume that the direction of Jw is only normal to the membrane's wall. The solution-diffusion is coupled with the transport equations by setting the vertical velocity on the membrane to be equal to Jw. So, equation (1) becomes $\nabla u = \pm Jw,$ where positive and negative signs donate the velocity at the upper and lower membranes, respectively, and equation (3) becomes$\nabla . (D_s \nabla u) - \nabla . (uc) = -Js.$

2.2The Film Theory

To develop a model incorporating proportional changes in velocity based on the concentration polarization (CP) layers as illustrated in **Fig**. **3**, it is crucial to understand the relation between the feed velocity and concentration polarization.

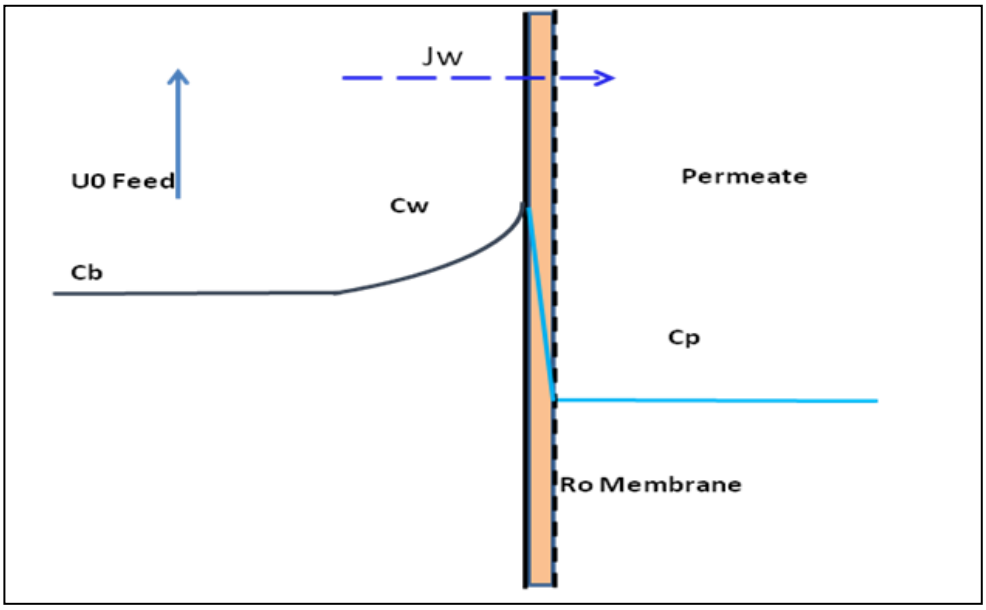

Fig. 3. Salt concentration profile in the membrane (concentration polarization)

The film model assumes one-dimensional flow and a fully-developed boundary layer [12, 13], which simplifies equations (2) and (3) to an ordinary differential equation, typically yielding an analytic solution as follows:

$$\frac{C_w - C_p}{C_b - C_p} = \exp\left(\frac{J_w}{K}\right) \tag{7}$$

Where C_w is the membrane surface concentration, *Cb* is the bulk concentration, and *K* is the mass transfer coefficient which can be estimated form an empirical correlation for laminar flow [14]

$$Sh = \frac{k\,d}{D} = 0.664 Re^{0.5}\, Sc^{0.33} \left(\frac{d}{L}\right)^{0.5} \tag{8}$$

Where Sh, Re, and Sc are Sherwood, Reynolds and Schmidt numbers, respectively and d is the hydraulic diameter, and L is the length.
Equations (7) and (8) indicate that increasing the mass transfer coefficient K leads to better mixing, and the salt concentration at the wall Cw approaches that of the bulk Cb. Furthermore, the mass transfer coefficient is directly proportional to the feed velocity. While an increase in the velocity magnitude destabilizes the concentration polarization, there exists an optimal velocity beyond which any further increase has a marginal impact on permeate production [15]. However, by increasing the velocity, especially at the membrane's end where scaling and

fouling are more likely to exist, the membrane's life span and productivity can be enhanced. This is a new variable which is not investigated in combination with other factors (feed spacer, permeably, concentration etc).

3. MODEL VALIDATION

Model validation against experimental results is a crucial step to ensure that the numerical model can produce realistic results under different operating conditions. an experimental study conducted on a cell test [14] **Fig. 4** and validated it using a 2D model. This study employs the published experimental data for validation. A 3D model was constructed based on the properties and geometry of the membrane is reported and presented in **Table 1** and **Fig. 4.** However, due to the uncertainty reported in the permeability values of the membrane, it is decided to simulate different scenario to reflect such uncertainty. Therefore, additionally to different operation conditions, the validation simulations run with maximum, minimum, and mean values of permeability. A combination of 3D and 2D models is employed to efficiently match experimental data. The 3D model matches selected points for accuracy, while the faster 2D model matches all data to reduce computation time. All simulation runs are solved by COMSOL 5.6, using laminar flow and transport of diluted species models. The governing equations are solved using direct fully coupled solver PARADISO. The error to reach conversion was set at $5x10^{-4}$.

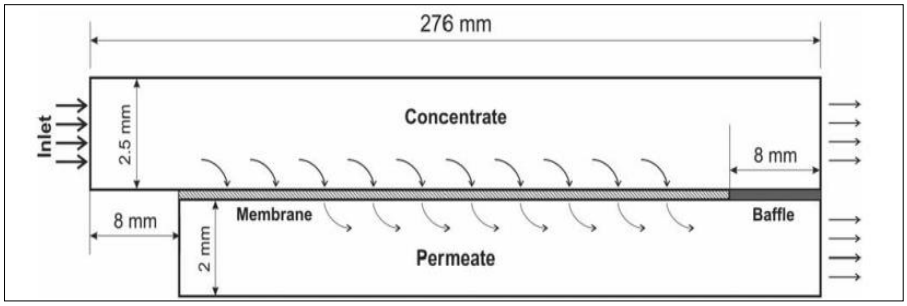

Fig. 4. Test cell geometry

Table 1 Membrane properties and operation condition

Item	Description	Value	Unites
K1	Hydraulic permeability	$6.93x10^{-7}$ ±0.33	m s^{-1} bar^{-1}
K2	Hydraulic permeability	$9.72x10^{-7}$ ±0.77	m s^{-1} bar^{-1}
R	Rejection factor	0.995	-
Ds	Diffusion coefficient	$1.5x10^{-9}$	m^3 / s
C_0	NaCl concentration	2	g l^{-1}
U_0	Inlet velocity	0.095 - 0.3	m s^{-1}
Δp	Operation pressure	9- 13	bar
K	Osmotic factor	4985	m^3 Pa /mol
W	Width	50	mm
H	Channel height	2.5	mm

3.1 3D Validation Results

The model in **Fig. 5** is fed with the properties in **Table 1**. The mesh consists of free tetrahedral elements and a boundary layer at the walls to better capture mass transportation and velocity profiles. The total number of elements is approximately 646000. The outlet pressure was set to 12 bar, and the inlet velocity was 0.095 m/s, as reported in experimental data. The permeating pressure was set to atmospheric. The simulated Jw value of 30 ($lm^{-2}.hr^{-1)}$ was

obtained, which is a very good match with the reported value of 30.9 ($lm\text{-}^{2}hr^{-1}$) with a feeble error of about 3%.

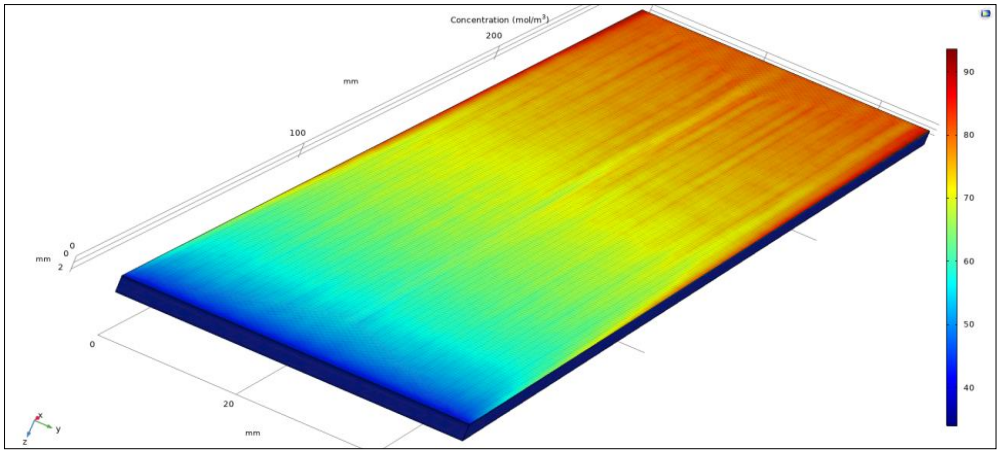

Fig. 5. 3D validation model, shows concentration at membrane wall increases towards the outlet

3.22 D Validation Results

The model is built using experimental data reported in **Table 1**. The 2D mesh consists of a triangular element and a boundary layer was set to walls. The total number of elements is 106860. The pressure was set to 9, 10, and 11 bar, and the inlet velocity was set to that of the experimental data. In addition, the permeability of the two membranes (K1 and K2) tested was also varied within the range of the reported measurement error as given in **Table 2**. The experimental results in the reference study were highly scattered, likely due to the variation in the membrane permeability caused by membrane compaction, as pointed out in the reference study.

Table 2. Permeability variation

Item	Mean	Minimum	Maximum
Membrane1 permeability (K1)	6.93×10^{-12}	6.60×10^{-12}	7.26×10^{-12}
Membrane2 permeability(K2)	9.72×10^{-12}	8.95×10^{-12}	1.05×10^{-11}

To improve the model's representativeness, we matched the trend of the experimental data. The overall model results showed good agreement with the experimental data as indicated in **Fig. 6**. The point-by-point errors were less than 15% for most data points, with a handful of outliers. This could be due to the high uncertainty in membrane permeability behavior and measurement errors.

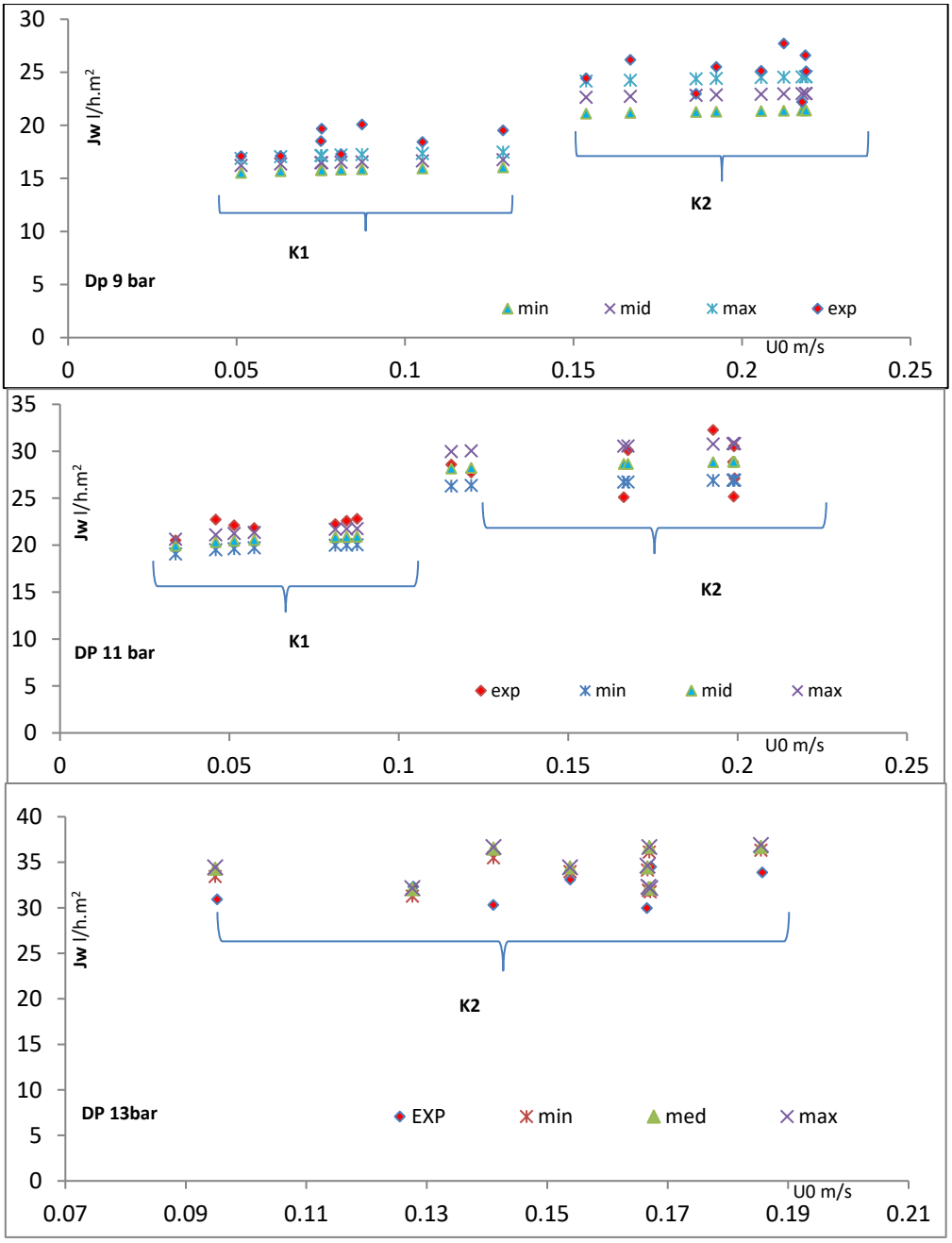

Fig. 6. Permeate flow (Jw) versus entry velocity (U0) at 9, 11, and 13 bar operational pressure of model Vs experimental results

4. THE BASE AND THE PROPOSED MODEL DEVELOPMENT

In order to increase the feed velocity proportionally to the length of the membrane, a modified width-to-length shape model, as depicted in **Fig. 7**, is developed. The performance of this modified shape model is then compared with that of a rectangular leaf shape model having the same membrane area. Usually the width to length ratio of the leaf in SW membranes is from 2 to 4 and sometimes 5 or more. A ratio of 2 is considered to keep the model size run-able on the work station used for this investigation. The entry velocity was varied based on Reynolds numbers of 100, 200, and 400. All other properties remain constant as presented in **Table 3**.

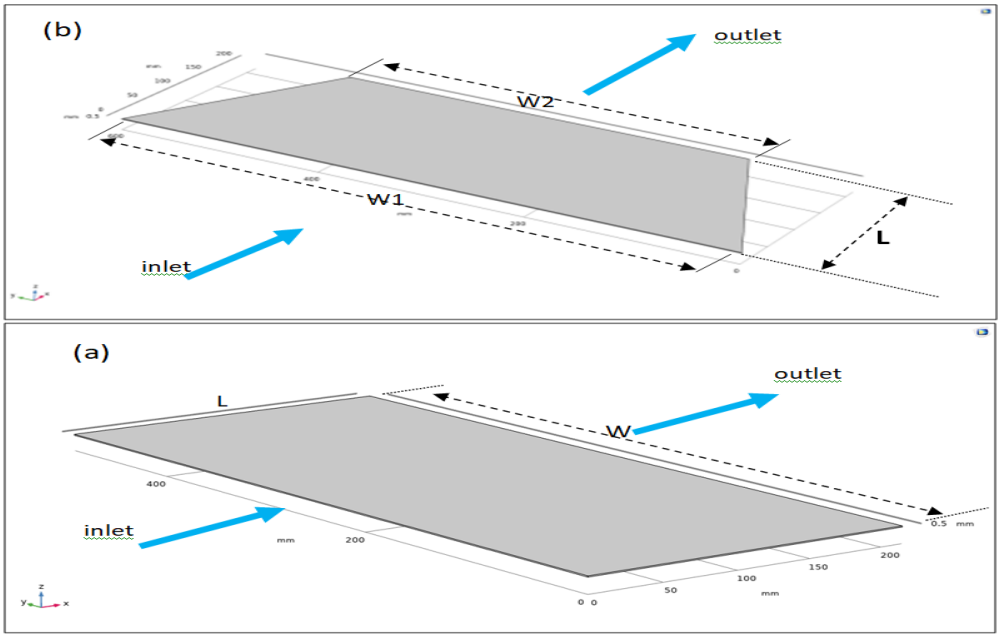

Fig. 7. Model geometry and orientation to feed flow (**a**) base case and (**b**) proposed cases

Table 3 Membrane properties and operation condition

Item	Description	Value	Units
K	Hydraulic permeability	$9.72x10^{-7}$	$m\ s^{-1}\ bar^{-1}$
R	Rejection factor	0.995	
Ds	Diffusion coefficient	$1.5x10^{-9}$	m^2 / s
C_0	NaCl concentration	2	$g\ l^{-1}$
U_0	Inlet velocity	0.05,0.1,0.2	$m\ s^{-1}$
Δp	Operation pressure	13	bar
k	Osmotic factor	4985	m^3 Pa /mol
W1	inlet Width	600	mm
W2	Outlet width	400	mm
L	Membrane length	215	mm
H	Channel height	1	mm
W	Width	500	mm

The model is discretized into tetrahedral elements of varying sizes, with denser meshes near the upper and lower membrane walls with a total number of elements of $9.5x10^6$ for both the proposed and base cases. A mesh refinement is implemented on membrane walls to ensure sufficient resolution in the mass transfer boundary layer.

5. THE SIMULATION RESULTS AND DISCUSSION

Key simulation results are presented in **Table 4**, where **U**in, **U**out, Pin, and Pout are inlet and outlet average feed velocities and pressures, respectively, **J**w is the permeate produced, Cw is the membrane surface concentration, and **J**w/(**P**in – **P**out) is the productivity.

Table 4: Simulation Results

	Uin (M/s)	Uout (M/s)	(Pin-Pout) (Pa)	Jw (m^3/s)x10^{-6}	Cw max mol/m^3	Cw mean mol/m^3	Jw / (Pin-Pout) x10^{-09}
Proposed	0.05	0.070	233.2	2.11	74.43	60.95	9.05
	0.1	0.145	557.2	2.17	72.95	55.12	3.89
	0.2	0.296	1233.3	2.22	70.24	50.37	1.80
Base case	0.05	0.046	168.4	2.09	77.64	62.54	12.4
	0.1	0.096	410.8	2.16	71.53	56.35	5.25
	0.2	0.196	915.3	2.21	66.05	51.13	2.41

5.1 Pressure Drop (Pin-Pout)

The proposed case shown in Fig. 8 consistently exhibits a higher pressure drop compared to the base case across all three scenarios. This is due to the congestion caused by the shape of the system, leading to increased resistance to the fluid flow. The pressure drop difference becomes more pronounced as the velocity of the fluid increases.

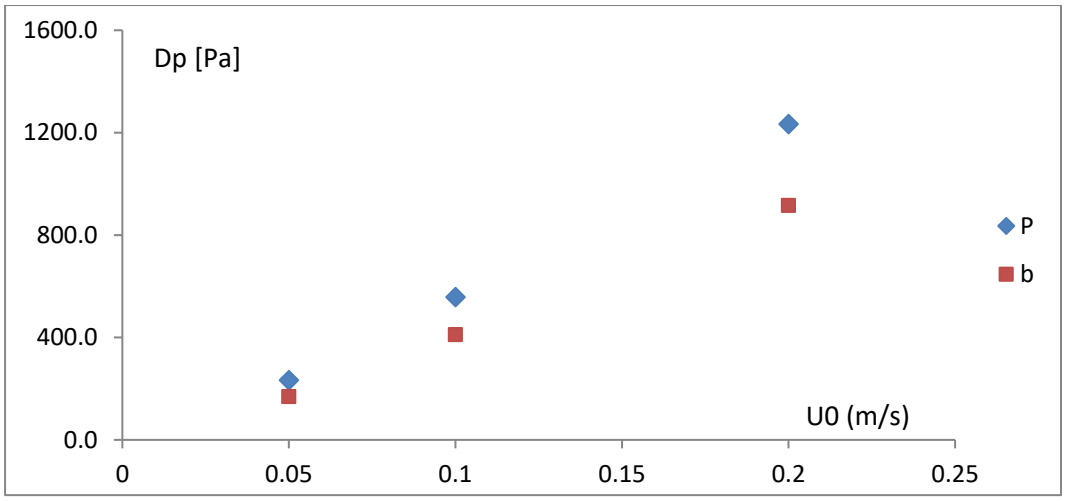

Fig. 8. Pressure drop (Dp) versus entry velocity (U0) for proposed (p) and base cases

5.2 Permeate Production (Jw)

While the proposed case in **Fig**. **9** shows a slightly higher permeate production, the base case demonstrates better productive performance (Jw/Pin-Pout), which is approximately 25% higher. This suggests that the base case is more efficient in converting the input pressure difference into productive output.

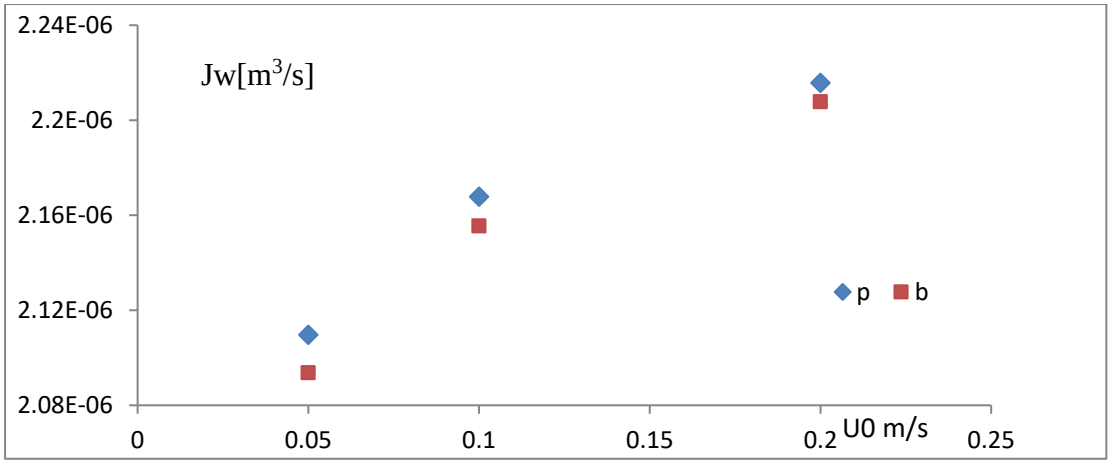

Fig. 9. Permeate production (Jw) versus entry velocity (U0) for proposed (p) and base case

5.3 Membrane Wall Surface Concentration (Cw)

As indicated in **Figs**. **10** and **11**, the base case scenario exhibits higher membrane wall surface concentration compared to the proposed case especially at the end of the membrane. However, this difference diminishes as the feed velocity increases. It implies that the proposed model generates higher velocities causing better mixing and reduces concentration polarization along the membrane surface.

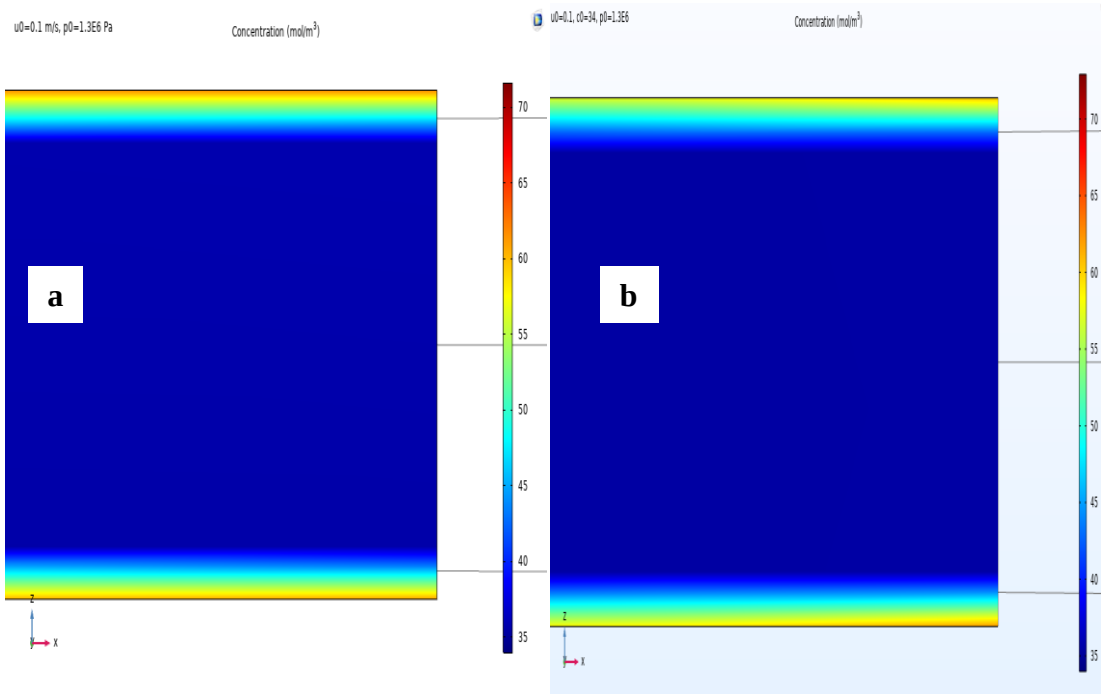

Fig. 10. Concentration polarization in (mol/m^3) for base case (a) and proposed case (b)

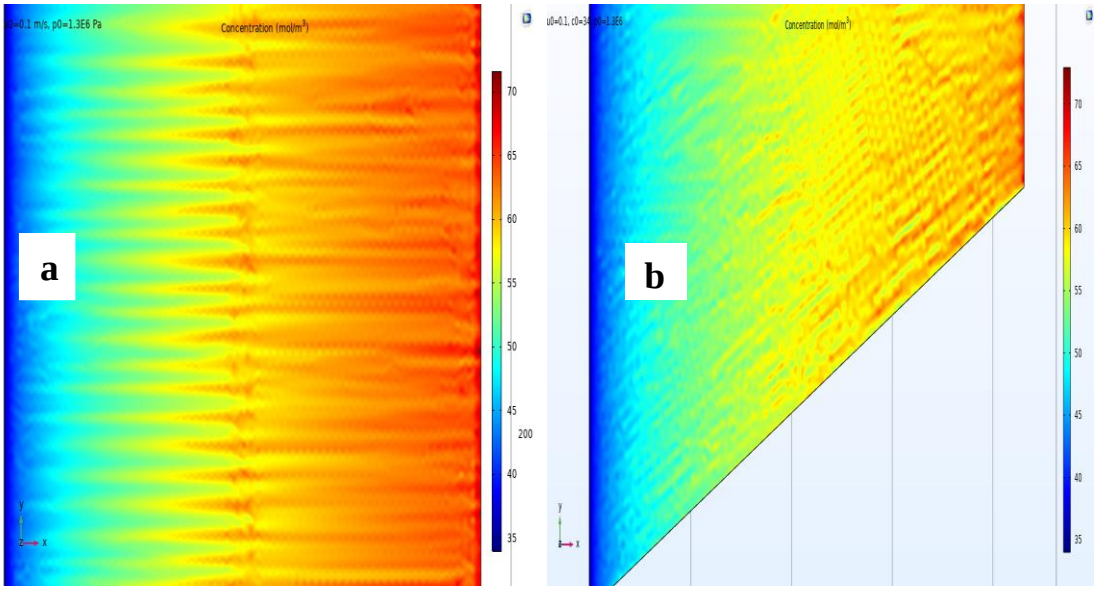

Fig. 11. Surface concentration in (mol/m3) for base case (a) and proposed case (b)

6. CONCLUSIONS

In this work, a novel design of an efficient spiral wound membrane is conducted. Computational fluid dynamics (CFD) is employed to examine the impact of altering the leaf shape in an empty channel on the feed velocity. The model is initially validated using experimental data available in the literature. Subsequently, the model is utilized to investigate the effects of this change at various Reynolds numbers. The findings suggest that the proposed model exhibits advantages at lower feed rates, as evidenced by the lower concentration achieved in this scenario, which indicates potential mitigation of scaling and fouling issues. And it would be interesting to consider other leaf shapes.

References

[1] Baker and W. Richard, Membrane Technology and Applications, 2nd ed, Newyork: John Wiley & Sons Ltd, 2004.

[2] Z. Cao, D. E. Wiley and A. G. Fane, "CFD simulations of net-type turbulence promoters in a narrow channel." J. Membr. Sci, 185, 157–176, 2001.

[3] A.Ahmad and K. Lau, "Impact of different spacer filaments geometries on 2D unsteady hydrodynamics and concentration polarization in spiral wound membrane channel," J. Membr. Sc,2006,286,77-92.

[4] C. Koutsou, S. Yiantsios and A. Karabelas, "Numerical and experimental study of mass transfer in spacer -filled channels: Effects of spacer geometrical characteristics and Schmidt number.," J. Membr. Sci. 2009, 326, 234–251.

[5] C. Koutsou, S.G., Yiantsios and K. A.J.A, "Direct numerical simulation of flow in spacer-filled channels: effect of spacer geometrical characteristics.," J. Membr. Sci. 2007, 291, 53–69..

[6] W. Wei, X. Zou, J. Xinxiang, R. Zhou, K. Zhao and Y. Wang, "Analysis of Concentration Polarization in Full-Size Spiral Wound Reverse Osmosis Membranes using Computational Fluid Dynamics," Membranes 2021, 11, 353., 2021.

[7] A. Qamar, S. Kerdi, J. S. Vrouwenvelder and N. Ghaffour, "Airfoil shaped filament feed spacer for improved filtration performance in water treatment," Scientific Reports 2023, 13, 10798.

[8] G. Shoukat, H. Idrees, M. Sajid, Y. A. Sara Ali, R. Nawaz and A. R. Ansari, "Numerical analysis of permeate flux in reverse osmosis by varying strand geometry," Scientific Reports 2022, 12,16636.

[9] G. Boram, A. C. S. and X. X. Yun, "The effect of feed spacer geometry on membrane performance and concentration polarisation based on 3D CFD simulations," Journal of Membrane Science,2017,527,78-91.
[10] M. SOLTANIEH and W. N. GILL, "review of reverse osmosis membranes and transport models," Chemical Engineering Communications, 12:4-6, 279-363, 1981.
[11] J. K., K. M.A. and K. M., "Mathematical modeling of reverse osmosis systems," Desalination,2004 ,160 ,29–42.
[12] H. Winston and K. Sirkar, Membrane Handbook, SPRINGER SCIENCE BUSINESS MEDIALLC,1992.
[13] M. Shakaib, S. Hasani and M. Mahmood, "CFD modelling for flow and mass transfer in spacer-obstructed membrane feed channels," Journal of Membrane Science,2009,326,270-284.
[14] A. Alexiadisa, D. Wileya, A. Vishnoib, R. Leea, D. Fletcherc and J. Baoa, "CFD modelling of reverse osmosis membrane flow and validation with experimental results," Desalination,2007,217,242-250.
[15] Haidari and Amir, "One Step Membrane Filtration A fundamental study," Delft University of Technology, 2017